Hindawi
Modelling and Simulation in Engineering
Volume 2024, Article ID 5676986, 11 pages
https://doi.org/10.1155/2024/5676986

Research Article

Enhanced Noise Suppression in Partial Discharge Signals via SVD and VMD with Wavelet Thresholding

Hailong Wang,[1] Yongliang Yao,[2] Guangdong Zhang,[1] Jidong Pan,[3] Longlong Gao,[3] Hai Jin ,[3] and Chuang Wang[4]

[1]*Electric Power Research Institute of State Grid Gansu Electric Power Company, Lanzhou 730000, China*
[2]*State Grid Gansu Electric Power Company, Lanzhou 730000, China*
[3]*College of Electrical Engineering and Information Engineering, Lanzhou University of Technology, Lanzhou 730000, China*
[4]*School of Electrical Engineering, Xi'an University of Technology, Xi'an 710048, China*

Correspondence should be addressed to Hai Jin; jinhai@lut.edu.cn

Received 31 October 2023; Revised 19 January 2024; Accepted 3 February 2024; Published 17 February 2024

Academic Editor: Angelos Markopoulos

Partial discharge evaluation is a principal method for assessing insulation conditions in power transformers. Traditional singular value decomposition (SVD) approaches, however, face issues like high residual noise and loss of signal details in white noise suppression. This article introduces an advanced denoising algorithm integrating SVD, variational mode decomposition (VMD), and wavelet thresholding to effectively address mixed noise in on-site power transformer assessments. The algorithm initially employs SVD to suppress mixed noise, specifically targeting narrowband interference by decomposing the noisy signal and nullifying the corresponding singular values. Post-SVD, the signal is further processed through VMD, with its modal components refined via wavelet thresholding. The final reconstruction of these denoised components effectively eliminates white noise. Applied to an input signal with a signal-to-noise ratio of -27.593 dB, the proposed method achieves a postdenoising ratio of 13.654 dB. Comparative analysis indicates its superiority over existing algorithms in mitigating white noise and narrowband interference and more accurately restoring the partial discharge signal.

1. Introduction

Power transformers are critical components within power systems, with their operational reliability being integral to the overall safety and stability of these systems. Empirical analysis of transformer malfunctions has identified insulation faults as the predominant factor impacting transformer functionality. Partial discharge (PD) diagnostic tests are a crucial tool for evaluating the insulation performance of transformers. However, PD signals, being inherently weak electrical signals, are susceptible to contamination from strong electromagnetic fields prevalent in transformers' high-voltage and high-current operational environments. Consequently, PD signals captured during on-site testing often encompass various forms of interference, such as white noise, periodic narrowband interference, and random pulse interference, leading to potential masking of PD signals within these interferences [1]. Such contamination can severely distort the PD waveform, adversely affecting the accuracy of fault diagnosis. Therefore, mitigating noise impact is essential for enhancing the precision of PD signal analysis and improving fault detection efficacy in practical scenarios.

Scholarly research has extensively explored various denoising methods for PD signals, such as fast Fourier transform (FFT) threshold filtering, empirical mode decomposition (EMD), wavelet thresholding, and singular value decomposition (SVD) [2]. Despite EMD's adaptability, it is hindered by mode mixing and endpoint effects, leading to suboptimal denoising [3]. To improve upon EMD, a method combining complete ensemble EMD with adaptive noise (CEEMDAN) and approximate entropy has been proposed, which, however, risks eliminating valid signals [4]. An adaptive SVD method is aimed at overcoming the limitations of manual singular value selection but struggles with complex signal reconstruction [5]. Fast SVD using Hankel matrices has shown promise in noise suppression in PD signals [6]. Improved variational mode decomposition (VMD) with threshold algorithms has been proposed for suppressing white noise and periodic narrowband interference, but it lacks precision in parameter selection [7]. A joint denoising approach using VMD and maximal overlap discrete wavelet packet transform (MODWPT) has been developed for rotating machinery vibration signals, but its efficacy in filtering both noise types is unspecified [8]. The flower pollination algorithm (FPA) has been used for parameter selection in VMD, followed by noise component removal with a Savitzky-Golay filter, albeit with slow convergence issues [9]. Optimizations of VMD through genetic algorithms have been explored for PD signal denoising, yet some lack the ability to mitigate narrowband interference [10, 11]. Curvature-based singular value transformation combined with empirical wavelet transform has been effective against white noise and narrowband interference, although threshold selection is prone to errors [12]. EMD-based decomposition with mutual information analysis for VMD suffers from EMD's inherent limitations [13]. An adaptive short-time SVD method for white noise demonstrates potential, but computational inaccuracies may impact its denoising effectiveness [14].

Aiming to enhance noise reduction efficacy, this article presents an advanced noise reduction methodology tailored to suppress mixed noise in PD signals, integrating SVD with VMD and optimized wavelet thresholding. Initially, a Hankel matrix representation of the noisy signal is employed, followed by the application of SVD to selectively eliminate narrowband interference, leveraging the distinct singular value profiles of PD and noise signals. Subsequent to the SVD process, the signal is decomposed using VMD. Enhanced wavelet thresholding is then applied to these modal components. The final step involves the reconstruction of these processed components, aiming to effectively remove white noise and suppress mixed noise within the PD signal framework. In Section 2, the detailed denoising algorithm is discussed, and simulation analysis is given in Section 3. Experimental signal validation is carried out in Section 4. Finally, conclusions are provided in Section 5.

2. Denoising Algorithm

The schematic diagram of the denoising algorithm for PD signals with mixed noise is shown in Figure 1. This section mainly introduces the basic theory of the denoising algorithm.

2.1. Singular Value Decomposition. The initial step necessitates the formation of a Hankel matrix [15].The construction is shown below: Let s be a noisy PD signal with noise. Transform s into a Hankel matrix as shown in the following equation.

$$A = \begin{bmatrix} s(1) & s(2) & \cdots & s(n) \\ s(2) & s(3) & \cdots & s(n+1) \\ \vdots & \vdots & & \vdots \\ s(m) & s(m+1) & \cdots & s(N) \end{bmatrix}. \quad (1)$$

Matrix A, with dimensions $m \times n$ and a rank of r, can be expressed as a product of an m-order orthogonal matrix U and an n-order orthogonal matrix V.

$$A = U\Sigma V^T, \quad (2)$$

where Σ is an $m \times n$-order diagonal matrix, with the first r orders having nonzero elements representing the singular values, and the rest are zeros [16]. The singular values corresponding to the noise components exhibit differences compared to the singular values of the original signal. By setting the singular values associated with noise to zero and retaining the singular values of the original signal, the process involves performing the inverse operation of SVD and reconstructing the signal to achieve denoising.

2.2. Variational Mode Decomposition. The solution of VMD consists mainly of two parts: the construction of the variational problem and its solution [17].

By estimating the signal's bandwidth, the variational constrained model is obtained as follows:

$$\begin{cases} \min\limits_{\{uk\},\{\omega k\}} \left\{ \sum_{k=1}^{K} \left\| \partial_t \left[\left(\delta(t) + \frac{j}{\pi t} \right) u_k(\mathrm{t}) \right] e^{-j\omega t} \right\|_2^2 \right\}, \\ \text{s.t.} \sum_{k=1}^{K} u_k = f, \end{cases} \quad (3)$$

where f is the noisy PD signal, u_k represents the K decomposed modal components, and ω_k denotes the center frequency of each decomposed modal component. $\delta(t)$ represents the unit impulse function.

Subsequently, we use the multiplier alternating direction algorithm to iteratively update the k intrinsic mode function (IMF) components and their respective center frequencies. The iterative formulas for modal components and center frequencies are shown in equations (4) and (5), respectively [18].

$$\widehat{u}_k^{n+1}(\omega) = \frac{\widehat{f}(\omega) - \sum_{i<k} \widehat{u}_i^{n+1}(\omega) - \sum_{i>k} \widehat{u}_i^{n+1}(\omega) + \widehat{\lambda}^n(\omega)/2}{1 + 2\alpha(\omega - \omega_k^n)^2}, \quad (4)$$

$$\omega_k^{n+1} = \frac{\int_0^\infty \omega \left| \widehat{u}_k^{n+1}(\omega) \right|^2 \mathrm{d}\omega}{\int_0^\infty \left| \widehat{u}_k^{n+1}(\omega) \right|^2 \mathrm{d}\omega}. \quad (5)$$

The iteration stops when the termination condition in equation (6) is satisfied, and k modal components are

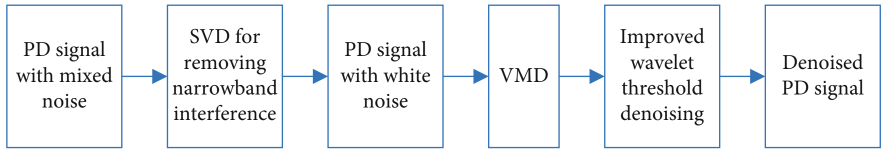

Figure 1: Schematic diagram of denoising mixed signals.

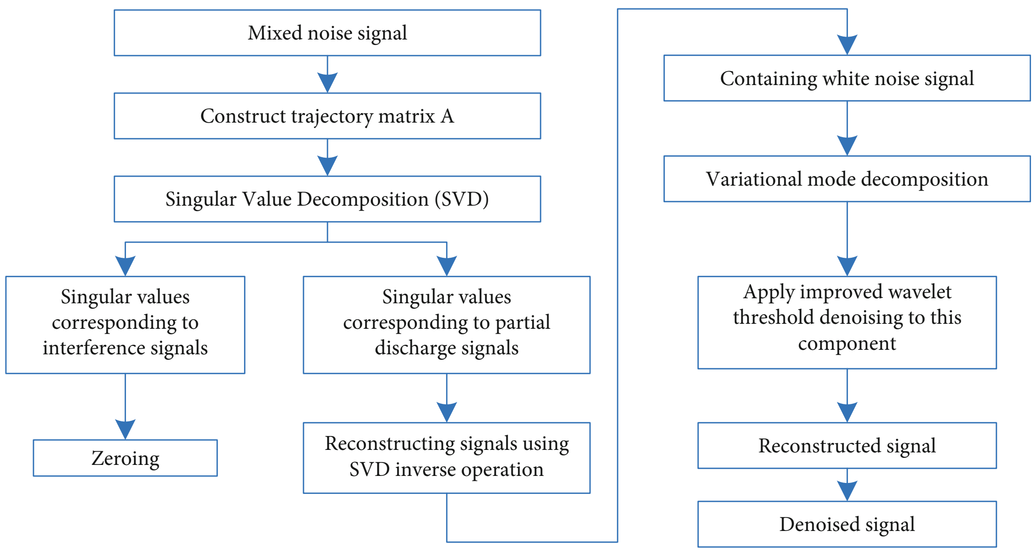

Figure 2: Algorithm denoising flowchart.

output, completing the decomposition. Here, ε represents the convergence accuracy.

$$\sum_k \frac{\left\|\widehat{u}_k^{n+1} - \widehat{u}_k^n\right\|_2^2}{\left\|\widehat{u}_k^n\right\|_2^2} < \varepsilon. \tag{6}$$

2.3. Wavelet Threshold Denoising. Wavelet threshold denoising entails the assessment of mathematical characteristics of wavelet coefficients, contrasting those between the target signal and the noise signal. Typically, the wavelet coefficients of the desired signal have larger amplitudes and concentrated energy, while those of the noise signal tend to have smaller amplitudes and more uniform energy distribution. Therefore, a specific threshold function can be set to distinguish between the desired signal and the noise signal [19].

The choice of threshold significantly affects the denoising effectiveness. Traditional threshold functions include hard thresholding and soft thresholding. Hard thresholding can lead to discontinuities in wavelet coefficients, resulting in reconstructed signals that lack the smoothness of the original signal. On the other hand, soft thresholding introduces a constant bias, distorting the reconstructed signal. To address the shortcomings of these traditional threshold functions, a refined threshold function is introduced, as illustrated in the following equation.

$$y_{j,k} = \begin{cases} \operatorname{sgn}\left(\omega_{j,k}\right) * \left(\omega_{j,k} - \dfrac{\lambda}{1+\alpha} * \gamma^{\sqrt{\omega_{j,k}^2 - \lambda^2}}\right), \left|\omega_{j,k}\right| > \lambda, \\ \operatorname{sgn}\left(\omega_{j,k}\right) * \dfrac{\alpha}{1+\alpha} * e^{10*\left(\left|\omega_{j,k}\right| - \lambda\right)} * \left|\omega_{j,k}\right|, \left|\omega_{j,k}\right| < \lambda. \end{cases} \tag{7}$$

Table 1: The parameters for the simulated PD signal, including amplitude, attenuation coefficient, and oscillation frequency.

PD pulse	Amplitude (A/mv)	Attenuation coefficient ($\tau/\mu s$)	Oscillation frequency (f_c/MHz)
1	10	0.1	20
2	5	0.15	40
3	10	0.1	20
4	5	0.15	40

This new function does not suffer from the fixed bias issues associated with soft and hard functions. By adjusting the tuning parameters α and λ, it can adapt to noise of varying intensities under different signal-to-noise ratio conditions.

Chang et al. [20] proposed a Bayes shrink method suitable for image denoising based on the distribution of two-dimensional wavelet coefficients. For a given parameter δ_x, it is necessary to find a threshold T that minimizes the Bayesian risk [21].

$$\begin{aligned} r(T) &= E(\tilde{x} - x)^2 = E_x * E_{x|y}(\tilde{x} - x)^2 \\ &= \iint (n(y) - x)^2 p(y|x) p(x) dy dx = \delta^2 * \omega\left(\frac{\delta_x^2}{\delta^2}, \frac{T}{\delta}\right). \end{aligned} \tag{8}$$

The threshold calculation expression is as follows [22]:

$$T_j = \frac{\delta^2}{\delta_x}. \tag{9}$$

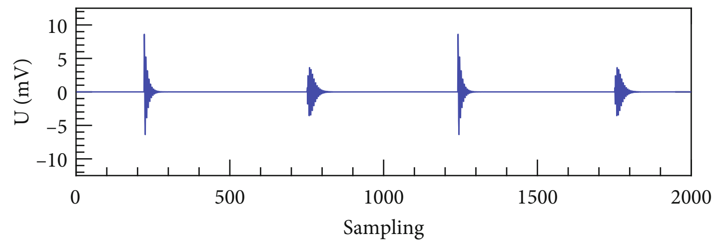

FIGURE 3: PD simulated signal.

In the above formula, δ^2 represents the variance of noise coefficients, and δ_x is the square root of the variance of sub-band coefficients. Here, j represents a specific decomposition level. The calculation for δ^2 is performed using the following equation [23]:

$$\bar{\delta} = \frac{\text{med}\left(\left|y_{j,k}\right|\right)}{0.6745}. \tag{10}$$

In this equation, $y(i)$ represents the coefficients of the noisy signal at different decomposition levels.

$$\bar{\delta} = \frac{1}{n}\sum_{i=1}^{n} y_{j,k}^2, \tag{11}$$

in which n represents the length of wavelet coefficients at each decomposition level, and it can be inferred from $\delta_y^2 = \delta_x^2 + \delta^2$:

$$\bar{\delta}_x = \sqrt{\max\left(\bar{\delta}_y^2 - \delta^2, 0\right)}. \tag{12}$$

Therefore, the threshold based on the Bayesian criterion can be determined through equations (10), (11), and (12). It is observed that the Bayesian threshold exhibits adaptability across different levels, overcoming the drawbacks of a fixed threshold.

2.4. Algorithm Steps. Based on the above theories, SVD is adopted in this paper to remove periodic narrowband interference, and VMD is combined with improved wavelet threshold denoising to remove white noise interference. The general flow chart is shown in Figure 2.

3. Simulation Analysis

3.1. Simulation Model. PD signals are characterized by their high-frequency nature, marked by rapid rising edges and durations typically spanning tens of nanoseconds. Due to the complexity of acquiring pure PD signals under practical field conditions, mathematical modeling is often employed to simulate these signals for theoretical analysis. Predominantly, four mathematical models are utilized for this purpose: the single exponential decay pulse model, the double exponential decay pulse model, the single exponential decay oscillation model, and the double exponential decay oscillation model, as referenced in [24, 25]. These models are mathematically formulated in the following equations.

TABLE 2: Parameters of the simulated periodic narrowband interference signal.

Narrowband interference	Amplitude (A/mV)	Frequency (f_i/MHz)
s_1	10	2
s_2	15	10
s_3	10	15

$$x_1(t) = A_1 e^{-(t-t_0)/\tau}, \tag{13}$$

$$x_2(t) = A_2\left(e^{-1.3(t-t_0)/\tau} - e^{-2.2(t-t_0)/\tau}\right), \tag{14}$$

$$x_3(t) = A_3 e^{-(t-t_0)/\tau} \sin\left(2\pi f_c (t - t_0)\right), \tag{15}$$

$$x_4(t) = A_4\left(e^{-1.3(t-t_0)/\tau} - e^{-2.2(t-t_0)/\tau}\right) \sin\left(2\pi f_c (t - t_0)\right), \tag{16}$$

where A signifies amplitude, τ the decay coefficient, f_c the oscillation frequency, and t_0 the initial pulse time.

For transformer PD signals, specific parameters of these models are detailed in Table 1, where pulses 1 and 3 align with single exponential decay oscillations and pulses 2 and 4 with double exponential decay oscillations. Figure 3 presents a visual representation of the simulated PD signal.

Periodic narrowband interference, characterized by a fixed resonant frequency, concentrated energy in the frequency domain, and a fixed phase distribution, is often simulated by superposing sinusoidal or cosinusoidal signals of varying frequencies and amplitudes [26]. The mathematical model for such interference is encapsulated in the following equation.

$$s_i = A_i \sum_{i=1}^{n} \sin(2\pi f_i t), \tag{17}$$

where A indicates the signal amplitude and f_i the frequency. The parameters for this model are listed in Table 2. Figure 4(a) demonstrates the PD signal with added narrowband interference, resulting in an SNR of -27.593 dB, which significantly obscures the original PD signal. Additionally,

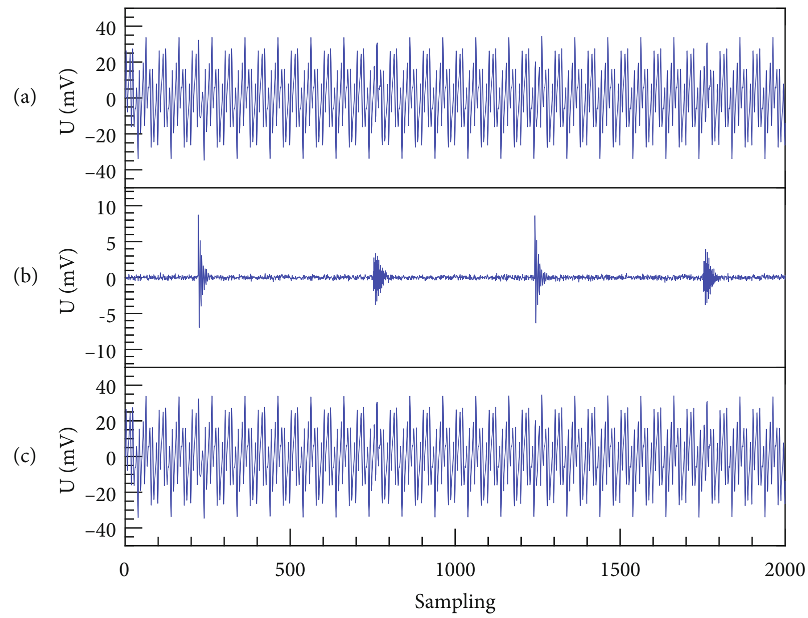

FIGURE 4: Time-domain plots of PD signals with interference. (a) PD signal with added narrowband interference. (b) PD signal with added white noise. (c) PD signal with both white noise and narrowband interference added.

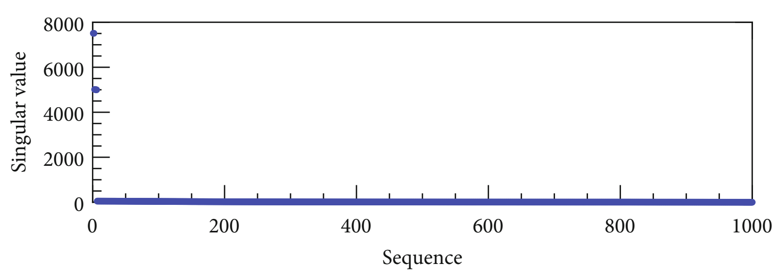

FIGURE 5: Singular value spectrum of signals with added narrowband interference.

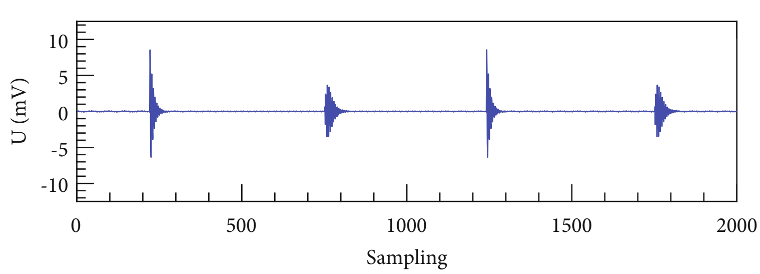

FIGURE 6: Signal after denoising periodic narrowband interference using SVD.

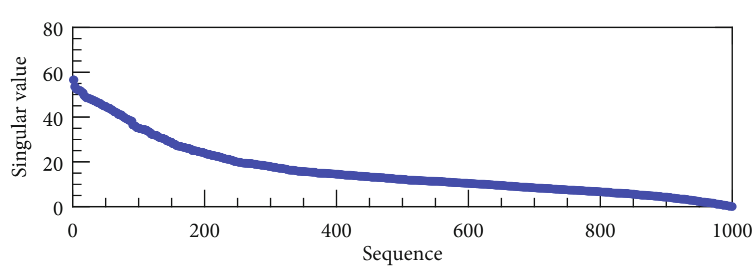

FIGURE 7: Singular value spectrum of PD signal with white noise interference.

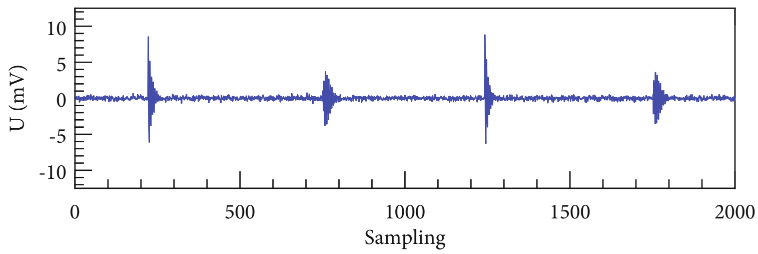

Figure 8: Localized discharge signal with white noise after SVD denoising.

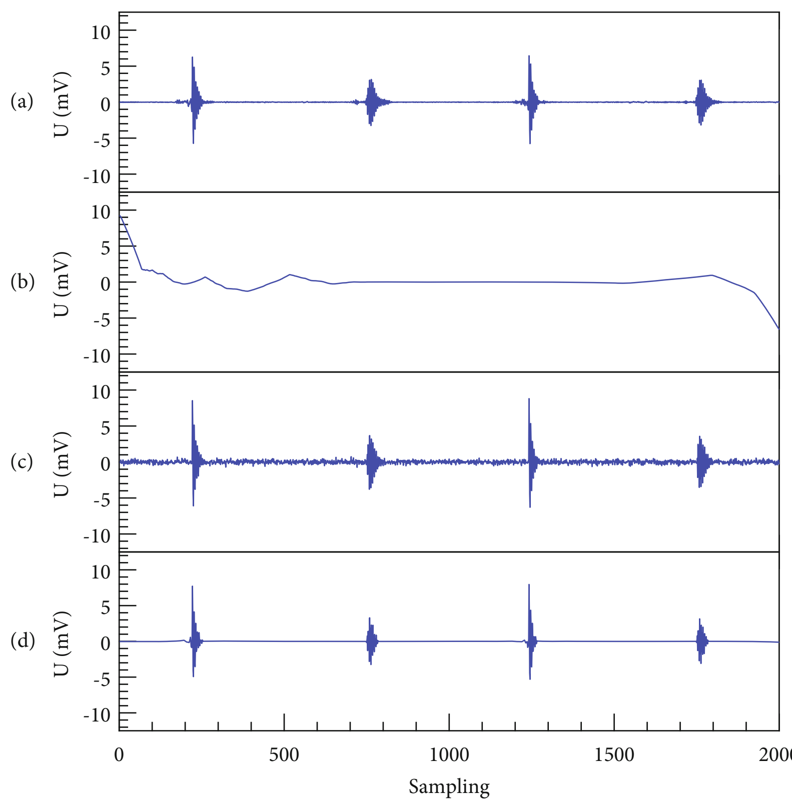

Figure 9: Denoising result comparison. (a) Denoising result using the method proposed in this paper. (b) Denoising result using wavelet thresholding. (c) Denoising result using SVD. (d) Denoising result using SVD combined with wavelet thresholding.

Gaussian white noise with a standard deviation of 0.2 is incorporated into the PD signal. Time-domain representations of the PD signal with added white noise and with both white noise and narrowband interference are exhibited in Figures 4(b) and 4(c), respectively.

The effectiveness of the denoising process is quantitatively assessed using three key metrics: signal-to-noise ratio (SNR), mean squared error (MSE), and normalized cross-correlation (NCC) [27]. In the context of the noisy signal analyzed above, the SNR was computed to be -27.593 dB, indicating the extent of noise prior to denoising. The MSE was calculated as 212.231, reflecting the initial discrepancy between the estimated and actual signal values. Additionally, the NCC was determined to be 0.047, illustrating the initial dissimilarity between the pre- and postdenoising signals.

Table 3: Parameters for evaluating denoising of PD simulated signals.

Denoising methods	SNR (dB)	NCC	MSE
Method of this paper	13.654	0.982	0.016
SVD	9.791	0.951	0.039
$SVD + WT$	11.156	0.975	0.028

3.2. Noise Reduction Processing

3.2.1. Using the SVD Method to Remove Narrowband Interference. Performing SVD on partial discharge signals superimposed with narrowband interference, Figure 5 illustrates the singular value spectrum of these signals. A notable observation from this spectrum is the clear distinction in the singular values corresponding to the narrowband

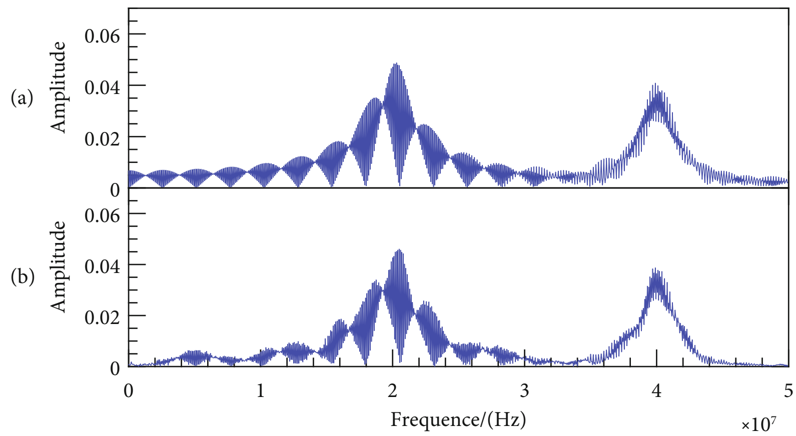

Figure 10: Signal spectrum comparison. (a) Spectrum of the original signal. (b) Spectrum of the denoised signal.

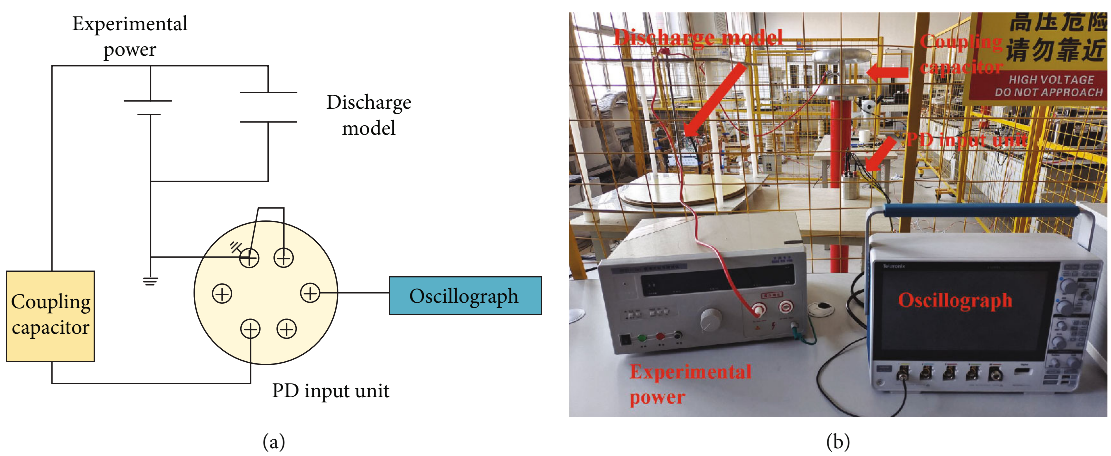

Figure 11: Experimental arrangement. (a) Experimental circuit diagram. (b) The connection of the experimental equipment.

interference, in contrast to those of the original PD signal. This distinction facilitates the identification and subsequent nullification of the singular values associated with the narrowband interference.

Subsequent to the annulment of singular values attributed to the periodic narrowband interference, Figure 6 portrays the resultant PD signal postremoval of this interference, employing SVD.

The computed metrics postdenoising are as follows: $SNR = 26.341\ dB$, $NCC = 0.998$, and $MSE = 8.581 \times 10^{-4}$. These values indicate that the periodic narrowband interference has been effectively mitigated.

Conducting singular value decomposition on the PD signal contaminated with white noise, the outcomes are depicted in Figure 7. It is evident that the singular values postdecomposition of the PD signal, which solely contains white noise, demonstrate substantial continuity with no distinct inflection points. This characteristic implies the unsuitability of SVD as a method for white noise elimination in such a scenario.

3.2.2. Denoising White Noise Using a Combination of VMD and Improved Wavelet Thresholding. In the context of simulated signals with mixed noise, the localized discharge signal post-SVD denoising is depicted in Figure 8. Following this process, the SNR is calculated to be 9.64 dB, indicating a notable enhancement in denoising effectiveness. The time-domain waveform after this treatment closely aligns with that of Figure 4(b), representing the PD signal with added white noise.

The signal processed using the proposed method, which combines VMD and improved wavelet thresholding subsequent to SVD, yields the denoised time-domain signal displayed in Figure 9(a). For comparative analysis, the PD signal containing both narrowband and white noise interference underwent processing through three distinct denoising methods: wavelet thresholding denoising, SVD denoising, and a combination of SVD and wavelet thresholding denoising, with outcomes illustrated in Figures 9(b)–9(d), respectively. Figure 9(b) presents the result post-wavelet thresholding denoising, revealing significant signal loss and minimal denoising effectiveness. Figure 9(c) exhibits the outcome of the SVD method, which effectively suppresses interference and retains discharge characteristics, though challenges in completely removing residual white noise persist. Figure 9(d) demonstrates the efficiency of the combined SVD and

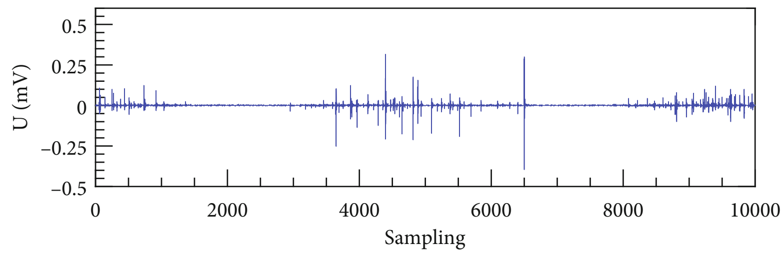

Figure 12: Measured PD signal for surface discharge.

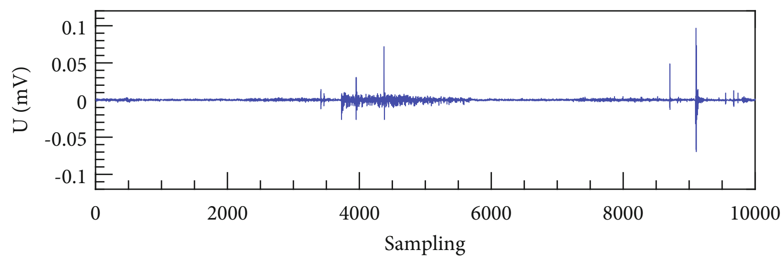

Figure 13: Measured PD signal for corona discharge.

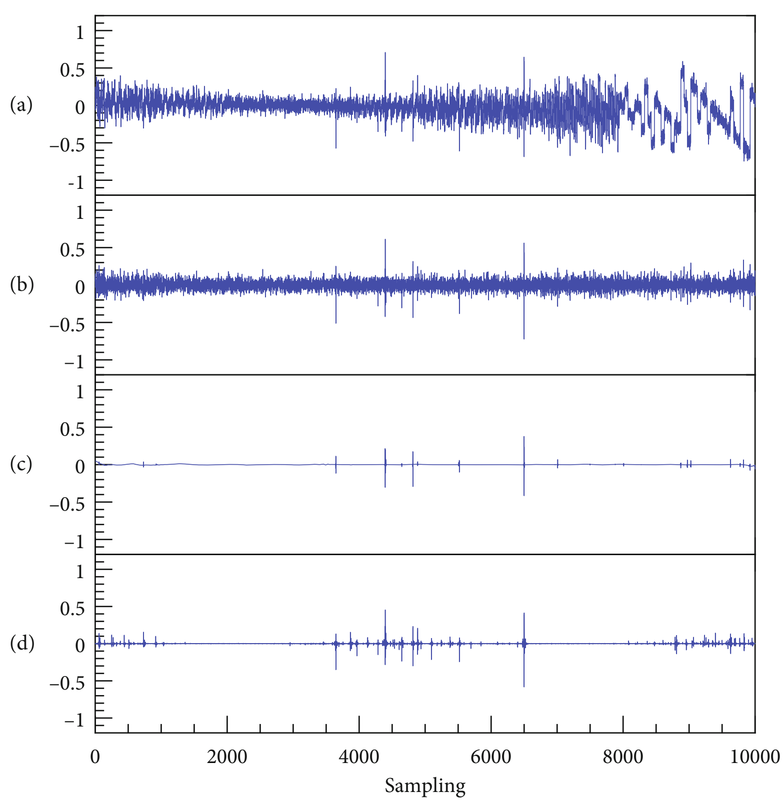

Figure 14: Comparison of denoising results for surface discharge. (a) Intentional noise addition. (b) Denoising result using SVD. (c) Denoising result using SVD combined with wavelet thresholding. (d) Denoising result using the method proposed in this paper.

wavelet thresholding method in suppressing both periodic narrowband and white noise interference, albeit with a slight diminution in partial discharge features.

Table 3 presents the results for three denoising evaluation parameters: SNR, NCC, and MSE, for the proposed method, the SVD method, and the combination of SVD and wavelet thresholding. The method introduced in this paper exhibits superior interference suppression and more effective waveform restoration.

Figure 10 facilitates a comparison between the spectral plots of the original and denoised signals. The spectral contents of both signals are remarkably similar, with only minor

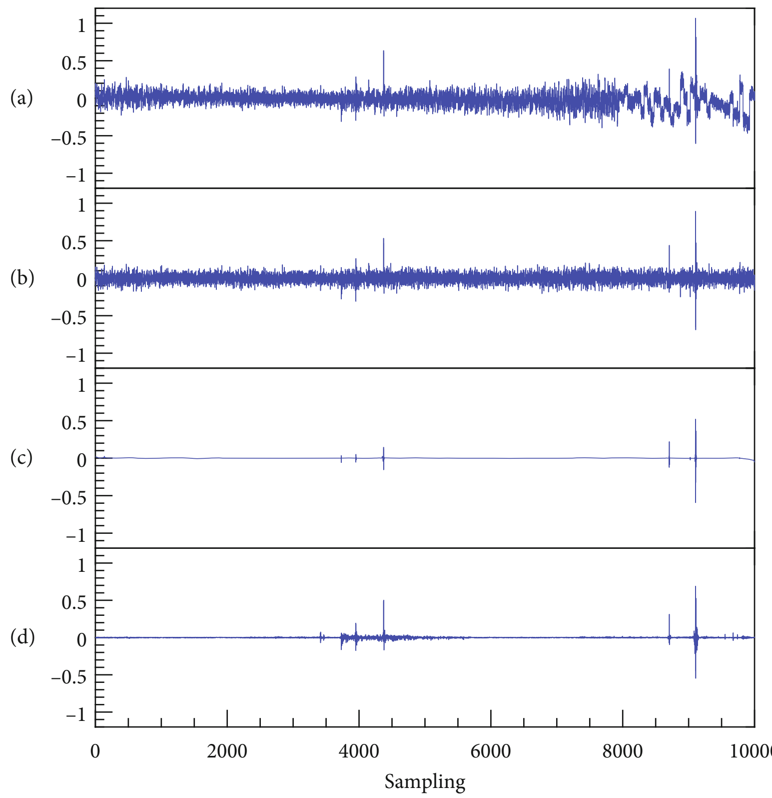

FIGURE 15: Comparison of denoising results for corona discharge. (a) Intentional noise addition. (b) Denoising result using SVD. (c) Denoising result using SVD combined with wavelet thresholding. (d) Denoising result using the method proposed in this paper.

TABLE 4: Measured parameters for denoised PD signals.

Denoising methods	PD signal	SVD	$SVD + WT$	Method of this paper
SNR	Surface discharge	-7.611	1.469	8.360
	Corona discharge	-11.204	2.115	7.802
MSE (10^{-3})	Surface discharge	0.934	0.115	0.023
	Corona discharge	0.098	0.004	0.001
NCC	Surface discharge	0.338	0.566	0.970
	Corona discharge	0.266	0.669	0.956

alterations observed in the primary peak regions, affirming the successful reduction of noise.

4. Denoising of Measured Signals

An empirical investigation was conducted in a laboratory environment to ascertain the performance of the proposed denoising method on real-world measured signals. The experimental setup comprised a discharge model, a coupling capacitor, a local measurement unit, a voltage withstand tester, and an oscilloscope. The configuration of this experimental arrangement is illustrated in Figure 11.

Figures 12 and 13 exhibit PD signals acquired in the laboratory setting for surface discharge and corona discharge, respectively. Given the minimal noise levels in these measured PD signals, they are treated as approximations of noise-free signals.

To further validate the method's efficacy, artificial noise was added to the signals for denoising analysis. Figures 14(a) and 15(a) illustrate the noisy PD signals, derived from collecting ambient laboratory noise under nondischarge conditions and the deliberate introduction of sinusoidal narrowband interference. These figures show that low-amplitude PD pulses are overwhelmed by the noise. Figures 14(b) and 15(b) demonstrate the results postdenoising using the SVD method, while Figures 14(c) and 15(c) display the outcomes following denoising with a combination of SVD and wavelet thresholding ($SVD + WT$). The denoising results using the proposed method are presented in Figures 14(d) and 15(d).

Table 4 lists the evaluation parameters for the actual measured signals. The proposed method not only augments the discernibility of PD features but also exhibits superior evaluation metrics compared to other methods. It effectively eliminates most interference noise, highlighting its proficient denoising effect.

In summary, our method demonstrates marked improvement in the visibility of PD features and excels in noise reduction, as evidenced by the denoising results and evaluation parameters for both surface and corona discharge signals.

5. Conclusions

This work introduces a denoising methodology that synergizes SVD and VMD with an enhanced wavelet thresholding technique, aimed at attenuating both periodic narrowband interference and white noise in PD signals. The efficacy of this integrated approach is validated through the analysis of both simulated and measured data, yielding several key findings:

(1) The singular values associated with periodic narrowband interference demonstrate specific distribution patterns. While SVD proves effective in attenuating this type of interference in PD signals, its performance in suppressing white noise interference is compromised, primarily due to challenges in accurately determining the threshold for singular values associated with white noise

(2) Wavelet transform, commonly employed in signal processing across diverse frequency ranges, may not efficiently capture the distinct frequency components characteristic of narrowband interference. This limitation potentially leads to less than optimal denoising outcomes

(3) The application of the refined thresholding method facilitates the adaptive adjustment of thresholds at varying scales, thereby enhancing the reduction of noise coefficients. This adaptability is particularly advantageous in addressing noise across different decomposition scales, improving the overall denoising efficiency

Data Availability

The data that support the findings of this study are available on request from the corresponding author, jinhai@lut.edu.cn, upon reasonable request.

Conflicts of Interest

The authors declare that they have no conflicts of interest.

Acknowledgments

This work was supported by the Gansu Provincial Natural Science Foundation of China (21JR7RA237) and Gansu Provincial Science and Technology Commissioner Special Project (22CX8GA11).

References

[1] Z. Jun, B. Xiaowen, S. Qin, C. Minwei, and Z. Dianbo, "Partial discharge signal denoising based on singular value decomposition and empirical wavelet transform," *IEEE Transactions on Instrumentation and Measurement*, vol. 69, no. 11, pp. 8866–8873, 2020.

[2] L. Linao and W. Xinlao, "Suppression method of partial discharge interferences based on singular value decomposition and improved empirical mode decomposition," *Energies*, vol. 14, no. 24, p. 8579, 2021.

[3] A. O. Boudraa, J. C. Cexus, and Z. Saidi, "EMD-based signal noise reduction," *International Journal of Signal Processing*, vol. 1, no. 1, pp. 33–37, 2004.

[4] S. Haikun, L. Yucai, J. Xu, Q. Bing, and Y. Jinliang, "A novel hybrid approach for partial discharge signal detection based on complete ensemble empirical mode decomposition with adaptive noise and approximate entropy," *Entropy*, vol. 22, no. 9, p. 1039, 2020.

[5] M. B. Ashtiani and S. M. Shahrtash, "Partial discharge denoising employing adaptive singular value decomposition," *IEEE Transactions on Dielectrics and Electrical Insulation*, vol. 21, no. 2, pp. 775–782, 2014.

[6] S. Govindarajan, J. Subbaiah, A. Cavallini, K. Krithivasan, and J. Jayakumar, "Partial discharge random noise removal using Hankel matrix-based fast singular value decomposition," *IEEE Transactions on Instrumentation and Measurement*, vol. 69, no. 7, pp. 4093–4102, 2020.

[7] X. Sa, C. Bo, D. Shen, and C. Hao, "Application of improved VMD and threshold algorithm in partial discharge denoising," *Journal of Electronic Measurement and Instrumentation*, vol. 35, pp. 206–214, 2021.

[8] Z. Xiaolong, X. Wang, H. Wang, X. Zhongyuan, Z. Yang, and C. Linlin, "Method for denoising the vibration signal of rotating machinery through VMD and MODWPT," *Sensors*, vol. 23, no. 15, p. 6904, 2023.

[9] J. Yang, Y. Ke, Z. Wang, and X. Zheng, "A novel denoising method for partial discharge signal based on improved variational mode decomposition," *Energies*, vol. 15, no. 21, p. 8167, 2022.

[10] Y. Wang, C. Peng, Z. Yongmei, and S. Yanying, "A denoising method for mining cable PD signal based on genetic algorithm optimization of VMD and wavelet threshold," *Sensors*, vol. 22, no. 23, p. 9386, 2022.

[11] Y. Deng, K. Zhu, G. Zhao, and J. Zhu, "Efficient partial discharge signal denoising method via adaptive variational modal decomposition for infrared detectors," *Infrared Physics and Technology*, vol. 125, article 104230, 2022.

[12] B. Xiaowen, Z. Jun, Z. Dakun, Z. Dianbo, and R. Ying, "Improved singular value and empirical wavelet decomposition algorithm in partial discharge denoising," *Power System Technology*, vol. 45, no. 12, pp. 4957–4963, 2021.

[13] R. Dhandapani, I. Mitiche, S. McMeekin, V. Mallela, and G. Morison, "Enhanced partial discharge signal denoising using dispersion entropy optimized variational mode decomposition," *Entropy*, vol. 23, no. 12, p. 1567, 2021.

[14] Z. Kai, L. Mingzhi, L. Yuan, M. Xie, and H. Yonglu, "An improved denoising method for partial discharge signals contaminated by white noise based on adaptive short-time singular value decomposition," *Energies*, vol. 12, no. 18, p. 3465, 2019.

[15] Y. Xu, J. Yan, Y. Wang, R. He, J. Wang, and G. Yingsan, "Novel denoizing method for partial discharge signals using singular value decomposition and spectral subtraction," *IET Science, Measurement & Technology*, vol. 17, no. 3, pp. 105–114, 2023.

[16] L. Qichang, B. Bing, and Z. Junyi, "A novel hierarchical situation awareness model for CBTC using SVD entropy and GRU with PRD algorithms," *IEEE Access*, vol. 9, pp. 132290–132300, 2021.

[17] K. Dragomiretskiy and D. Zosso, "Variational mode decomposition," *IEEE Transactions on Signal Processing*, vol. 62, no. 3, pp. 531–544, 2014.

[18] Z. Wang, G. He, D. Wenhua et al., "Application of parameter optimized variational mode decomposition method in fault diagnosis of gearbox," *IEEE Access*, vol. 7, pp. 44871–44882, 2019.

[19] J. Lu, H. Lin, Y. Dong, and Z. Yansheng, "A new wavelet threshold function and denoising application," *Mathematical Problems in Engineering*, vol. 2016, Article ID 3195492, 8 pages, 2016.

[20] S. G. Chang, Bin Yu, and M. Vetterli, "Adaptive wavelet thresholding for image denoising and compression," *IEEE Transactions on Image Processing*, vol. 9, no. 9, pp. 1532–1546, 2000.

[21] Y. Qingming, C. Mingmin, and S. Min, "Improved wavelet denoising method for infrared image application," *Computer Engineering and Applications*, vol. 52, no. 1, pp. 173–177, 2016.

[22] S. Ruikar and D. Doye, "Image denoising with modified wavelet feature restoration," *International Journal of Computer Science Issues (IJCSI)*, vol. 9, no. 2, p. 403, 2012.

[23] D. L. Donoho, "De-noising by soft-thresholding," *IEEE Transactions on Information Theory*, vol. 41, no. 3, pp. 613–627, 1995.

[24] S. Kang, Z. Jing, S. Wenwen, and J. Guo, "Extraction of partial discharge pulses from the complex noisy signals of power cables based on CEEMDAN and wavelet packet," *Energies*, vol. 12, no. 17, p. 3242, 2019.

[25] J. Tang, G. Li, X. Yanbin, C. Jiao, and Z. Xiaoxing, "Suppressing PD's periodicity narrow band noise in the PD measurement by using complex wavelet packet transform," *High Voltage Engineering*, vol. 11, pp. 2355–2361, 2008.

[26] X. Luo, N. Haiqing, R. Hu, L. Fang, and W. Juzhuo, "A modified method of suppressing narrow-band interference using fast Fourier transform power spectrum," *Proceedings of the CSEE*, vol. 33, no. 12, 2013.

[27] L. Zhipeng, F. Wang, and L. Chuanyang, "A denoising method of partial discharge signal based on improved SVD-VMD," *IEEE Transactions on Dielectrics and Electrical Insulation*, vol. 30, no. 5, pp. 2107–2116, 2023.